

Deflected Talbot-Mediated Overtone Spectroscopy in Near-Infrared as a Label-Free Sensor on a Chip

Aviad Katiyi and Alina Karabchevsky*

Cite This: *ACS Sens.* 2020, 5, 1683–1688

Read Online

ACCESS |



Metrics & More



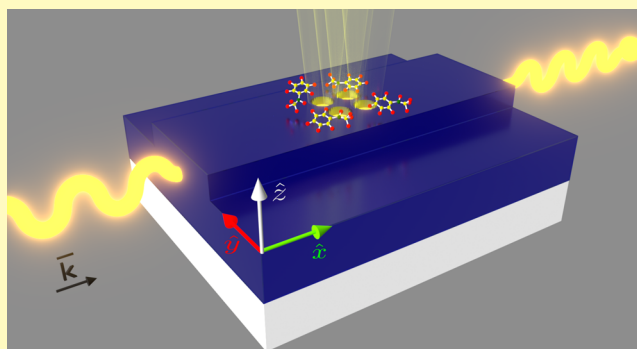
Article Recommendations



Supporting Information

ABSTRACT: Rapid, sensitive, and reliable detection of aromatic amines, toxic manufacturing byproducts, has been previously achieved with molecular vibrations in the mid-infrared (Mid-IR) region. However, Mid-IR spectroscopic tools are hampered by a need to prepare the samples and the sensor cost. Here, we develop an affordable label-free sensor on a chip, operating in near-infrared (NIR) for ultrasensitive detection of absorption line signatures based on molecular vibrations overtones of the aromatic amine *N*-methylaniline probe molecule. We design a perforated silicon rib waveguide and fabricate it by milling cylindrical inclusions through the waveguide core. The molecular signatures were monitored when waveguides are embedded in toxic *N*-methylaniline, experiencing a deflected Talbot effect. We observed that when the Talbot effect is deflected, the absorption lines in NIR are enhanced despite the weakly absorbing nature of the probe molecules. This new spectroscopic strategy can potentially be extended to detect other common toxic byproducts in a chip-scale label-free manner and to enhance the functionality of chemical monitoring.

KEYWORDS: molecular overtones, optical waveguide, multimode interference, near-infrared spectroscopy, integrated photonics



Multimode interference (MMI) devices have attracted growing interest in integrated optics^{1,2} widely used for a variety of applications such as communication,^{3,4} optical spectroscopy,⁵ and integrated photonics.^{6,7} MMI devices have a characteristic Talbot pattern. This pattern was discovered in 1836 by Talbot⁸ in a periodic structure such as diffraction grating, which creates a self-imaging effect. By illuminating a diffraction grating, Talbot observed repetition of color bands. Later, in 1881, this effect was rediscovered and explained by Rayleigh.⁹ When light passes through the periodic diffraction grating, it creates an image of the grating at distance z_T , which is named the Talbot length. The Talbot effect also occurs in multimode (MM) waveguides.^{10–12} However, in the MM waveguides, the Talbot effect is related to the different propagation constants of the guided modes but not to the periodicity of the input source. When a guided wave is transmitted through a multimode optical waveguide, it creates wavefront replicates of a periodic perturbation pattern along the propagation direction of the guided wave.¹³ This occurs due to the multimode interference effect. The MMI effect is used to minimize and improve the optical devices, such as Mach–Zehnder switches^{14,15} and modulators,¹⁶ and to enhance the functionality of integrated photonic circuits.

Our sensor is based on the MMI effect. It is important to note that MMI-based devices such as optical couplers have low propagation losses and allow for small device dimensions,¹³ which make them ideal for Mach–Zehnder interferometers¹⁷

and other integrated photonic components. In addition, the multimode interference effect in a waveguide can be used for sensing applications.¹⁸ A sensor based on MMI can achieve a resolution of 5.41×10^{-5} RIU.¹⁹ Instead of using the MMI effect on a slab waveguide, the MMI structure can be also created out of slot waveguides. Due to the changes in the refractive index inside the slot, the output then is changed, leading to the resolution of 9.8×10^{-5} RIU.²⁰ However, those structures behave as refractometers, which essentially lack in specificity. In contrary, spectrometers operating in low energies in infrared are specific since they are able to identify a molecular structure from the unique absorption lines.²¹ Despite the fundamental interest to understand the mechanism of absorption by molecular vibrations overtones, the probability of the overtone transition of $\Delta\nu > 1$ (ν is the number of the energy level) is very small. The overtone absorption is an order of magnitude smaller compared to the fundamental vibration absorption,²² which makes the detection of the overtone absorption challenging.^{23–25}

Received: February 19, 2020

Accepted: May 8, 2020

Published: May 8, 2020



Here, we study the deflected Talbot effect realized in a weakly absorbing molecular medium. To understand the mechanism underlying the deflected Talbot effect in a weakly absorbing medium, we combined several disciplines, namely, the physics of guided wave optics, the waveguide with inclusions fabrication routines, the surface chemistry, and the molecular overtone spectroscopy. We explore the overtone absorption by multimode interference (MMI) in multimode silicon rib waveguides and reveal that the deflected Talbot effect increases the probability of overtone transitions. Next, we investigate the influence of cylindrical inclusions in the guiding layer on the Talbot effect.

EXPERIMENTAL SECTION

Numerical Simulation. We built the three-dimensional (3D) model and performed simulations using a commercial Maxwell solver: Lumerical FDTD (finite difference time domain) solutions. A Gaussian beam, with a wavelength of 1.5 μm , radius of 4.75 μm , and divergence angle of 0.13 rad, was launched into a silicon-on-insulator (SOI) rib waveguide with a slab height of 1.6 μm , strip height of 0.4 μm , width of 8 μm , and waveguide length of 30 μm . The refractive indices of silicon and silica are $n_{\text{Si}}(1.5 \mu\text{m}) = 3.48$ and $n_{\text{SiO}_2}(1.5 \mu\text{m}) = 1.444$, respectively. The waveguide was embedded in *N*-methyl aniline ($n_{\text{NMA}}(1.5 \mu\text{m}) = 1.5712 + i8.931 \times 10^{-5}$)¹⁸ in a distance of 10 μm from the input facet. The cross section of the electric field in x - y and x - z planes was taken in the middle of the waveguide, $y = 0$ and $z = 1 \mu\text{m}$, respectively.

Waveguide Fabrication. The rib waveguide was fabricated on silicon-on-insulator (SOI) wafer (Si carrier, 2 μm SiO₂ and 2 μm Si). For the fabrication process, we used e-beam resist poly-methyl methacrylate (PMMA) 950K for writing the waveguides. After writing and developing the resist, we evaporated a hard mask of aluminum with a thickness of 50 nm via an electron gun evaporator. Next, we soaked the sample in acetone for 4 h as the lift-off process, and we cleaned the sample with isopropanol (IPA). Eventually, we dry-etched the sample with SF₆ + Ar and O₂, which enables us to get a straight line and 90° waveguide wall. We removed the residue of the Al using a 400K developer.

Inclusion Cluster Fabrication. The inclusions of cylindrical shape were milled into the silicon guiding layer using a Helios focused ion beam (FIB). The holes were fabricated with a depth of 2 μm and radius of 0.58 μm .

Spectroscopy on a Waveguide. A broadband laser source (Fianium WL-SC-400-15), with bandwidths of 450 to 2400 nm, was focused into a single mode fiber (1550BHP) using a X10 plan achromat objective (Olympus) with a numerical aperture of NA = 0.25. The single-mode fiber was aligned to the waveguide using a 3D stage (3-Axis NanoMax Stage) and monitored by a stereo microscope (Zeiss Stemi SV6) for precise alignment. The transmitted spectra were collected using a multimode fiber into an optical spectrum analyzer (Yokogawa 6370D) at a wavelength range of 1–1.7 μm and resolution of 1 nm.

RESULTS AND DISCUSSION

Molecular Overtone Transitions. Molecular vibration overtone transitions can be excited in near-IR. Each molecular vibration transition has a different probability to occur, which is expressed by the oscillator strength. The oscillator strength f is proportional to the square of electric dipole transition moment²⁶

$$f = \left(\frac{4\pi m_e \nu_{ij}}{3e^2 \hbar} \right) |\mu_{ij}|^2 \quad (1)$$

where m_e is the mass of an electron, \hbar is the reduced Planck constant, ν_{ij} is the frequency for transition from state i to state

j , and μ_{ij} is the electric dipole transition moment, which is defined as

$$\mu_{ij} = \langle i | \mu | j \rangle = \int \psi_i^* \mu \psi_j \, d\mathbf{r} \quad (2)$$

where ψ is the wave function. The electric dipole moment μ is defined as

$$\mu = \mu_0 + \left(\frac{\partial \mu}{\partial r} \right)_0 r + \frac{1}{2} \left(\frac{\partial^2 \mu}{\partial r^2} \right)_0 r^2 + \dots \quad (3)$$

where μ_0 is the dipole moment at $r = 0$, where r is the displacement and 0 indicates that the derivatives are at the equilibrium bond length (detailed description of oscillator strength can be found in the Supporting Information). From eq S-10 in the Supporting Information, one can see that the probability of the overtone vibration is an order of magnitude smaller compared to the probability fundamental vibration,²² which makes it hard to identify. For this reason, here, we propose to enhance the overtone transition probability by the induced deflected Talbot effect on perforated optical waveguides with inclusions of cylindrical shape.

To investigate the influence of the inclusions on the Talbot effect, we study a Silicon-On-Insulator (SOI) nanostrip rib waveguide with 5 nm Ta₂O₅ overlayer, which acts as a capping layer, having a cluster made of cylindrical inclusions in the guiding layer, which is shown in Figure 1. We choose a square

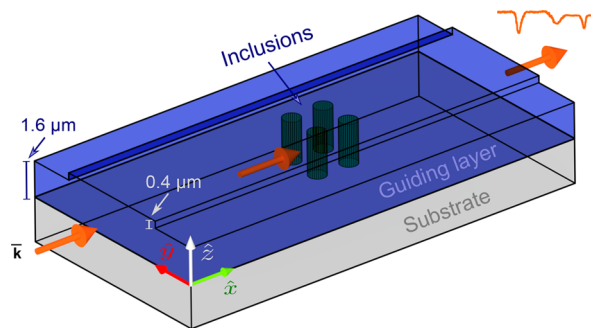


Figure 1. Schematic of the dielectric rib waveguide with a silicon guiding layer on the silica substrate with a cluster of inclusions of cylindrical shape.

configuration for the hole cluster due to the growing interest of quadrumers for different fundamental phenomena.²⁷ A cylindrical shape was chosen for the inclusions due to the easy fabrication process compared to other shapes. To observe the Talbot effect by a multimode interference, we modeled the waveguide with a height of 1.6 μm , nanostrip height of 400 nm, and inclusion diameter of 1.12 μm , as shown in Figure 1.

Using Lumerical FDTD software, we modeled the waveguide when the inclusions are embedded in different media: air and weakly absorbing media of *N*-methyl aniline (NMA) molecule.²⁸ A Gaussian beam, with a wavelength of 1.5 μm , radius of 4.75 μm , and divergence angle of 0.13 rad, was launched into the waveguide. The inclusions were engraved at a distance of 20 μm from the input facet. We explored the conditions for the deflected Talbot regime in x - y and x - z waveguide planes and its influence on molecular overtone transitions. Due to the propagation of a number of modes in a multimode waveguide, a wavefront replicates the periodic perturbation pattern along the propagation. When the dielectric perturbation occurs in a waveguide, some of the

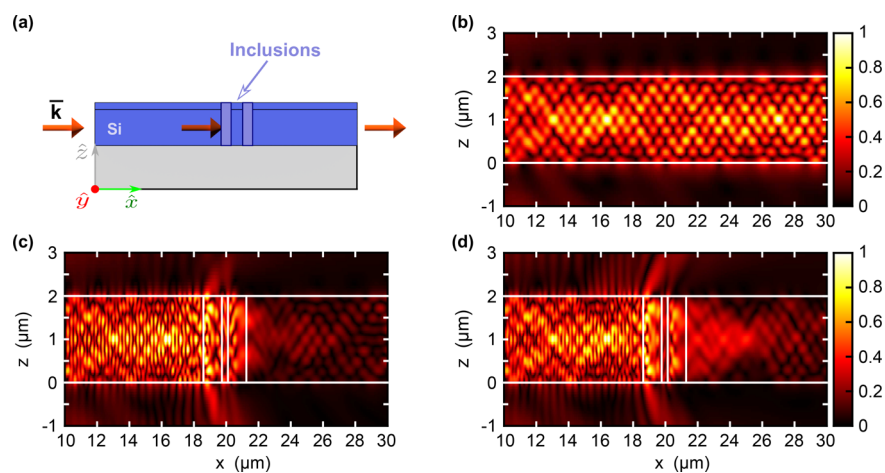


Figure 2. (a) Schematic of the cross section in the center of the waveguide, x - z plane ($y = 0 \mu\text{m}$). Evolution of the electric field when the waveguide was embedded in (b) air without inclusions, (c) air with inclusions, and (d) N -methylaniline, $n_{\text{NMA}} = 1.5712 + i8.931 \times 10^{-5}$, with inclusions.

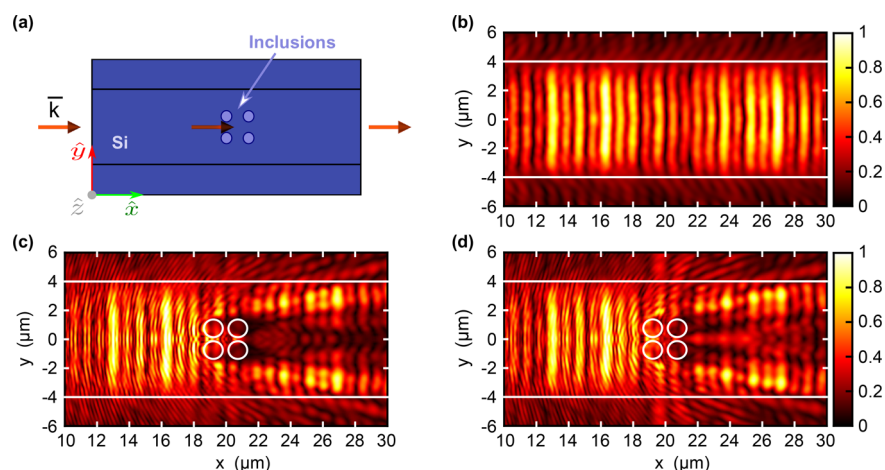


Figure 3. (a) Schematic of the cross section in the center of the waveguide, x - y plane ($z = 1 \mu\text{m}$). Evolution of the electric field when the waveguide was embedded in (b) air without inclusions, (c) air with inclusions, and (d) N -methylaniline, $n_{\text{NMA}} = 1.5712 + i8.931 \times 10^{-5}$, with inclusions.

power transfers to other modes, which creates the deflected Talbot effect.

First, we investigated the influence of the inclusions at the x - z plane of the waveguide. Figure 2a shows a schematic cross section in the center of the waveguide at the x - z plane. Due to the multimode interference, a self-imaging Talbot effect occurs in the silicon rib waveguide (Figure 2b). When the cylindrical inclusion cluster is placed inside the core, the deflected Talbot effect (Figure 2c,d) occurs when the guiding layer is embedded in air and in weakly absorbing medium with dispersion of N -methylaniline,^{24,28} respectively, which creates perturbation along the propagation direction of the waveguide. Next, we investigated the influence of the inclusions at the x - y plane of the waveguide. Figure 3a shows a schematic cross section in the center of the waveguide at the x - y plane. Figure 3b shows the Talbot effect in the silicon rib waveguide as a deformation of the field along the propagation. A perturbation appears along the propagation direction in the waveguide (Figure 3c,d) caused by the introduced inclusion cluster in the guiding layer embedded in air and in N -methylaniline, respectively. We notice a leakage beyond the waveguide strip confinement. Figures 2 and 3 show that some power transfers to the other

modes and the Talbot effect becomes deflected due to the dielectric perturbation of cylindrical shape (the evolution of the guided modes is shown in the Supporting Information).

For the experiment, we first fabricated and characterized the silicon rib waveguides. Figure 4a shows a scanning electron micrograph image of fabricated rib waveguides (top view) without inclusions. Next, the Talbot effect was deflected by the cylindrical inclusion cluster milled into the guiding layer with a focused ion beam (FIB) with a depth of $2 \mu\text{m}$ and radius of 580 nm . Figure 4b shows a scanning electron micrograph image of the zoomed area on the fabricated inclusion cluster (top view). The waveguides were characterized and tested using the inline waveguide measurement setup, as described in Experimental Section. Figure 4c shows a photograph of the inline setup with a fiber in-coupled rib waveguide aligned on the 3D stage. Fiber-out is collecting the output signal from the waveguide into the optical spectrum analyzer (OSA) (not shown).

To further explore the influence of the deflected Talbot regime on the overtone molecular absorption on the waveguide, we constructed the experimental setup shown in Figure 5a. We used red light of 80 mW . Therefore, partially,

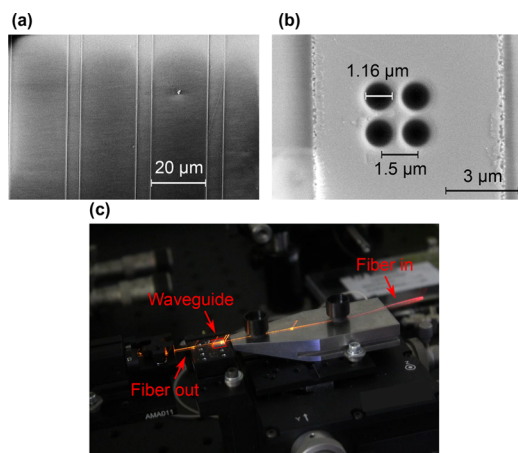


Figure 4. (a) Scanning electron microscopy (SEM) image of the rib waveguide. (b) Scanning electron microscopy (SEM) image of the fabricated inclusions on the rib waveguide. (c) Photograph of the inline experimental setup.

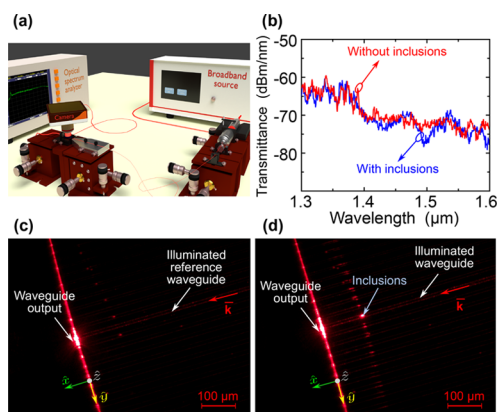


Figure 5. (a) Artistic impression of the experimental setup. (b) Measured transmittance spectra with OSA on the reference waveguide (red curve) and on the waveguide with a cylindrical inclusion cluster (blue curve). Note, both waveguides were embedded in *N*-methylamine medium. Top view of the waveguides captured with an optical microscope. (c) Reference waveguide. (d) Waveguide with fabricated inclusions.

such high-power light can be guided in the waveguide. It allows for the visualization of the waveguide lines and facilitates the alignment. Next, a broadband laser source was coupled to a single-mode fiber (SMF1550). The fiber was placed on a piezo-electric stage for precise and accurate inspection. The output signal was collected by a multimode fiber into an optical spectrum analyzer (OSA). We dropped 12 μL of *N*-methylamine onto the inclusion cluster shown in Figure 4c, resulting in the spectrum shown in Figure 5b (blue curve). For comparison, the laser was coupled to the reference waveguide (with no inclusions) with *N*-methylamine, resulting in the spectrum shown in Figure 5b (red curve). Figure 5c,d shows the upper view of the illuminated waveguide.

Figure 5b shows the transmittance spectrum of *N*-methylamine on the rib waveguide with and without inclusions at a broad wavelength range of 1.3–1.6 μm . The absorption of the N–H bond in *N*-methylamine is clearly seen around 1.5 μm on the waveguide with the inclusions. The absorption of *N*-methylamine when dripped onto the waveguide surface and filled in the inclusions is approximately

3.5 dB compared to dripped *N*-methylamine on a waveguide without the inclusions. It shows that in the deflected Talbot regime caused by the inclusions, we enhance the absorption effect of the *N*-methylamine probe molecule. Figure 5d shows the far-field scattering effect caused by the cylindrical inclusions compared to the scattering in the reference waveguide, as shown in Figure 5c, which fits the simulation results shown in Figure 3b,d.

We noticed that dielectric perturbations such as cylindrical holes enhance the absorption when the hole diameter is comparable to the incident wavelength. This can be explained by the scattering effect.

2D Scattering from a Cylinder Embedded in the Waveguide Core. The enhanced absorption of *N*-methylamine overtones can be explained by the multiple scattering events.^{28,29} One can explain the resonant elastic scattering of light by a chain of coherent absorption and re-emission events. Simply put, the photons are re-emitted in random directions because the wave vector is not conserved by the system for the lack of translational symmetry. The resonant scattering results in a significant increase in the mean trajectory of photons travelling through the guide. However, the actual scattering of a waveguide mode by a finite cylinder with a height of $H \approx \lambda$ and diameter of $D \approx \lambda$ cannot be solved analytically. Therefore, for describing the scattering effect by cylinders in the waveguide core, we will ignore the height restriction of the cylinder and illuminate it with a planar wave.

In the case of TE mode when the electric field is parallel to the xz plane, the scattered fields of a single cylinder (shown in Figure 6a) are defined as³⁰

$$\mathbf{E}_s = - \sum_{n=-\infty}^{\infty} E_n [b_{nl} \mathbf{N}_n^{(3)} + ia_{nl} \mathbf{M}_n^{(3)}] \quad (4)$$

$$\mathbf{H}_s = i \frac{k}{\omega \mu} \sum_{n=-\infty}^{\infty} E_n [b_{nl} \mathbf{M}_n^{(3)} + ia_{nl} \mathbf{N}_n^{(3)}] \quad (5)$$

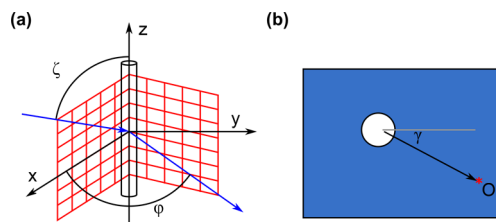


Figure 6. (a) Long cylinder illuminated by a plane wave. (b) Top view of the cylindrical hole.

where $E_n = E_0 (-i)^n / (k \sin \zeta)$, and $\mathbf{M}_n^{(3)}$ and $\mathbf{N}_n^{(3)}$ are the proper cylindrical vector harmonics,³⁰ which are given by

$$\mathbf{M}_n^{(3)} = \nabla \times (\hat{z} \psi_n) \quad (6)$$

$$\mathbf{N}_n^{(3)} = \frac{\nabla \times \mathbf{M}_n}{k} \quad (7)$$

where ψ_n is the generation function, which is defined as

$$\psi_n = H_n^{(1)}(kr \sin \zeta) e^{in\varphi} e^{-ikz \cos \zeta} \quad (8)$$

where k is the wavenumber and $H_n^{(1)}$ is the Hankel function of the first kind, $H_n^{(1)} = J_n + iY_n$.

Using the continuity equations for E and H at the cylinder boundary ($r = a$), we obtain the two coefficients

$$a_{nl} = \frac{C_n V_n - B_n D_n}{W_n V_n + i D_n^2}$$

$$b_{nl} = \frac{W_n B_n + i C_n D_n}{W_n V_n + i D_n^2}$$

where the auxiliary functions are defined as

$$B_n = \xi [m^2 \xi J'_n(\eta) J_n(\xi) - \eta J_n(\eta) J'_n(\xi)]$$

$$C_n = n \cos(\zeta) J_n(\eta) J_n(\xi) \left(\frac{\xi^2}{\eta^2} - 1 \right)$$

$$D_n = n \cos(\zeta) \eta J_n(\eta) H_n^{(1)}(\xi) \left(\frac{\xi^2}{\eta^2} - 1 \right)$$

$$W_n = i \xi [\eta J_n(\eta) H_n^{(1)'}(\xi) - \eta H_n^{(1)}(\xi) J'_n(\eta)]$$

$$V_n = \xi [m^2 \xi J'_n(\eta) H_n^{(1)'}(\xi) - \eta H_n^{(1)'}(\xi) J_n(\eta)]$$

and

$$\xi = ka \sin \zeta \quad \eta = ka \sqrt{m^2 - \cos^2(\zeta)}$$

where m is the relative refractive index of the medium filling the cylinder ($m = \frac{n_n + i\kappa_n}{n_{\text{wg}}}$), and a is the cylinder radius.

In the case of a waveguide, the incident illumination is at normal incident to the inclusions ($\zeta = 90^\circ$); hence, a_{nl} is equal to zero. Therefore, b_{nl} can be calculated as

$$b_{nl} = \frac{J_n(mx) J'_n(x) - m J'_n(mx) J_n(x)}{J'_n(mx) H_n^{(1)'}(x) - m J'_n(mx) H_n^{(1)}(x)} \quad (9)$$

For a finite cylinder, the correction factor is given by³¹ $f_c = \frac{2 \sin(kLA)}{kLA}$, where $A = \cos \zeta + \sin \theta \cos \phi$ and L is half of the cylinder length. This factor provides the spectral correction that depends on the cylinder length. However, it does not consider a space dependence of the field along the cylinder axes.

Using this simplified model, we can estimate the effect of the inclusion cluster. Using a single scattering model, the scattered field at an arbitrary point O is described as the sum of scattered field of each hole.

$$\mathbf{E}_{s(t)} = \sum_{n=1}^4 \mathbf{E}_{sn}(\gamma_n, |\mathbf{r}_O - \mathbf{r}_n|) \quad (10)$$

where n is the hole number and γ_n is the angle from the hole to point O .

The scattered field $\mathbf{E}_{s(t)}$ from the whole cluster of inclusions leads to the enhanced absorption when the hole diameter is comparable to the incident wavelength. The scattering transfers energy to the high-order modes, which have larger interaction with the surrounding. The scattering enhances the sensitivity of the waveguide, allowing us to identify the unique absorption lines of the molecule.

CONCLUSIONS

In conclusion, we have presented a waveguide system experiencing the deflected Talbot effect due to the appearance

of perturbations of cylindrical shape in the waveguide core embedded in weakly absorbing medium *N*-methylaniline.²⁸ We fabricated the waveguides on the SOI platform and milled inclusions in them using the FIB technique. We found that the deflected Talbot effect on a waveguide enhances the absorption of molecular transition overtones. Specifically, the absorption line of the N–H bond of *N*-methylaniline excited around 1.5 μm experienced a drop of 3.5 dB as compared to unperturbed by the inclusion waveguide. In addition, we noticed that dielectric perturbations such as cylindrical holes enhance the absorption when the hole diameter is comparable to the incident wavelength due to the scattering effect. This paves the way for integrated spectrometers in which the enhancement of the weak absorption occurs due to the perturbation in the waveguide core.

ASSOCIATED CONTENT

Supporting Information

The Supporting Information is available free of charge at <https://pubs.acs.org/doi/10.1021/acssensors.0c00325>.

Oscillator strength of overtones and fundamental modes, evolution of guided mode, and Figures S-1–S-4 (PDF)

AUTHOR INFORMATION

Corresponding Author

Alina Karabchevsky – School of Electrical and Computer Engineering and Ilse Katz Institute for Nanoscale Science & Technology, Ben-Gurion University of the Negev, Beer-Sheva 8410501, Israel; orcid.org/0000-0002-4338-349X; Email: alinak@bgu.ac.il

Author

Aviad Katiyi – School of Electrical and Computer Engineering and Ilse Katz Institute for Nanoscale Science & Technology, Ben-Gurion University of the Negev, Beer-Sheva 8410501, Israel; orcid.org/0000-0002-7924-9065

Complete contact information is available at: <https://pubs.acs.org/doi/10.1021/acssensors.0c00325>

Notes

The authors declare no competing financial interest.

ACKNOWLEDGMENTS

This work has been supported by Israel Innovation Authority within KAMIN program Grant No. 69073. The authors acknowledge Dr. Joseph Gurwich for fruitful discussion.

REFERENCES

- (1) Yin, R.; Jiang, X.; Yang, J.; Wang, M. Structure with improved self-imaging in its graded-index multimode interference region. *J. Opt. Soc. Am. B* **2002**, *19*, 1301–1303.
- (2) Khalil, D.; Yehia, A. Two-dimensional multimode interference in integrated optical structures. *J. Opt. Soc. Am. B* **2003**, *6*, 137.
- (3) Ota, M.; Sumimura, A.; Fukuhara, M.; Ishii, Y.; Fukuda, M. Plasmonic-multimode-interference-based logic circuit with simple phase adjustment. *Sci. Rep.* **2016**, *6*, 24546.
- (4) Lierstuen, L.; Sudbo, A. 8-channel wavelength division multiplexer based on multimode interference couplers. *IEEE Photonics Technol. Lett.* **1995**, *7*, 1034–1036.
- (5) Wan, N. H.; Meng, F.; Schröder, T.; Shiue, R.-J.; Chen, E. H.; Englund, D. High-resolution optical spectroscopy using multimode interference in a compact tapered fibre. *Nat. Commun.* **2015**, *6*, 7762.

- (6) Peruzzo, A.; Laing, A.; Politi, A.; Rudolph, T.; O'Brien, J. L. Multimode quantum interference of photons in multiport integrated devices. *Nat. Commun.* **2011**, *2*, 224.
- (7) Geints, Y. E.; Minin, O. V.; Minin, I. V.; Zemlyanov, A. A. Self-images contrast enhancement for displacement Talbot lithography by means of composite mesoscale amplitude-phase masks. *J. Opt. Soc. Am. B* **2020**, *22*, No. 015002.
- (8) Talbot, H. F. LXXVI. Facts relating to optical science. No. IV. *London Edinburgh Phil. Mag. J. Sci.* **1836**, *9*, 401–407.
- (9) Rayleigh, L. *London Edinburgh Phil. Mag. J. Sci.* **1881**, *11*, 196–205.
- (10) Bryngdahl, O. Image formation using self-imaging techniques. *J. Opt. Soc. Am.* **1973**, *63*, 416–419.
- (11) Ulrich, R. Light-propagation and imaging in planar optical waveguides. *Nouv. Rev. Opt.* **1975**, *6*, 253.
- (12) Praxmeyer, L.; Wódkiewicz, K. Talbot effect in cylindrical waveguides. *Opt. Commun.* **2006**, *268*, 215–225.
- (13) Soldano, L. B.; Pennings, E. C. M. Optical multi-mode interference devices based on selfimaging: principles and applications. *J. Lightwave Technol.* **1995**, *13*, 615–627.
- (14) Bachmann, M.; Smit, M.; Besse, P.; Gini, E.; Melchior, H.; Soldano, L. Polarization-insensitive low-voltage optical waveguide switch using InGaAsP/InP four-port Mach-Zehnder interferometer. In *Conference on Optical Fiber Communication/International Conference on Integrated Optics and Optical Fiber Communication*; OSA Publishing: 1993, p TuH3.
- (15) Agrawal, N.; Weinert, C.; Ehrke, H.-J.; Mekonnen, G.; Franke, D.; Bornholdt, C.; Langenhorst, R. Fast 2 x 2 Mach-Zehnder optical space switches using InGaAsP-InP multi-quantum-well structures. *IEEE Photonics Technol. Lett.* **1995**, *7*, 644–645.
- (16) Zucker, J.; Jones, K.; Chiu, T.; Tell, B.; Brown-Goebeler, K. Strained quantum wells for polarization-independent electrooptic waveguide switches. *J. Lightwave Technol.* **1992**, *10*, 1926–1930.
- (17) Jenkins, R. M.; Devereux, R. W. J.; Heaton, J. M. A novel waveguide Mach-Zehnder interferometer based on multimode interference phenomena. *Opt. Commun.* **1994**, *110*, 410–424.
- (18) Katiyi, A.; Karabchevsky, A. Si Nanostrip Rib-Waveguide for On-Chip Broadband Molecular Overtone Spectroscopy in Near-Infrared. *ACS Sensors* **2018**, *3*, 618–623.
- (19) Wang, J.; Jin, Y.; Zhao, Y.; Dong, X. Refractive index sensor based on all-fiber multimode interference. *Optik* **2013**, *124*, 1845–1848.
- (20) Mayeh, M.; Viegas, J.; Srinivasan, P.; Marques, P.; Santos, J. L.; Johnson, E. G.; Farahi, F. Design and fabrication of slotted multimode interference devices for chemical and biological sensing. *J. Sen.* **2009**, *2009*, 1.
- (21) Katiyi, A.; Zorea, J.; Halstuch, A.; Elkabets, M.; Karabchevsky, A. Surface roughness-induced absorption acts as an ovarian cancer cells growth sensor-monitor. *Biosens. Bioelectron.* **2020**, *161*, 112240.
- (22) Stuart, B. *Infrared spectroscopy: Fundamentals and applications*; John Wiley & Sons, Ltd.: Sussex, 2004.
- (23) Struve, W. S. *Fundamentals of molecular spectroscopy*; Wiley: New York, 1989.
- (24) Katiyi, A.; Karabchevsky, A. Figure of merit of all-dielectric waveguide structures for absorption overtone spectroscopy. *J. Lightwave Technol.* **2017**, *35*, 2902–2908.
- (25) Borovkova, O. V.; Ignatyeva, D. O.; Sekatskii, S. K.; Karabchevsky, A.; Belotelov, V. I. High-Q surface electromagnetic wave resonance excitation in magnetophotonic crystals for super-sensitive detection of weak light absorption in the near-infrared. *Photonics Res.* **2020**, *8*, 57–64.
- (26) Atkins, P. W.; Friedman, R. S. *Molecular quantum mechanics*; Oxford University Press: 2011.
- (27) Terekhov, P. D.; Evlyukhin, A. B.; Redka, D.; Volkov, V. S.; Shalin, A. S.; Karabchevsky, A. Magnetic Octupole Response of Dielectric Quadrumers. *Laser Photonics Rev.* **2020**, 1900331.
- (28) Karabchevsky, A.; Kavokin, A. V. Giant absorption of light by molecular vibrations on a chip. *Sci. Rep.* **2016**, *6*, 21201.
- (29) Karabchevsky, A.; Katiyi, A.; Bin Abdul Khudus, M. I. M.; Kavokin, A. V. Tuning the Near-Infrared Absorption of Aromatic Amines on Tapered Fibers Sculptured with Gold Nanoparticles. *ACS Photonics* **2018**, *5*, 2200–2207.
- (30) Bohren, C. F.; Huffman, D. R. *Absorption and scattering of light by small particles*; John Wiley & Sons: 2008.
- (31) Hulst, H. C.; van de Hulst, H. C. *Light scattering by small particles*; Courier Corporation: 1981.